

A simple regulatory architecture allows learning the statistical structure of a changing environment

Stefan Landmann,¹ Caroline M. Holmes,² and Mikhail Tikhonov³

¹*Institute of Physics, Carl von Ossietzky University of Oldenburg, D-26111 Oldenburg, Germany*

²*Department of Physics, Princeton University, Princeton, NJ 08544, USA*

³*Department of Physics, Center for Science & Engineering of Living Systems, Washington University in St. Louis, St. Louis, MO 63130, USA*

(Dated: January 5, 2021)

Bacteria live in environments that are continuously fluctuating and changing. Exploiting any predictability of such fluctuations can lead to an increased fitness. On longer timescales bacteria can “learn” the structure of these fluctuations through evolution. However, on shorter timescales, inferring the statistics of the environment and acting upon this information would need to be accomplished by physiological mechanisms. Here, we use a model of metabolism to show that a simple generalization of a common regulatory motif (end-product inhibition) is sufficient both for learning continuous-valued features of the statistical structure of the environment and for translating this information into predictive behavior; moreover, it accomplishes these tasks near-optimally. We discuss plausible genetic circuits that could instantiate the mechanism we describe, including one similar to the architecture of two-component signaling, and argue that the key ingredients required for such predictive behavior are readily accessible to bacteria.

Keywords: Fluctuating environments | Metabolic regulation | Learning

Organisms that live in changing environments evolve strategies to respond to the fluctuations. Many such adaptations are reactive, e.g. sensory systems that allow detecting changes when they occur, and responding to them. However, adaptations can be not only reactive, but also predictive. For example, circadian clocks allow photosynthetic algae to reorganize their metabolism in preparation for the rising sun [1, 2]. Another example is the anticipatory behavior in *E. coli*, which allows it to prepare for the next environment under its normal cycling through the mammalian digestive tract [3]; similar behaviors have been observed in many species [4, 5].

All these behaviors effectively constitute predictions about a future environment: the organism improves its fitness by exploiting the regularities it “learns” over the course of its evolution [6]. Learning such regularities can be beneficial even if they are merely statistical in nature. A prime example is bet hedging: even if the environment changes stochastically and without warning, a population that learns the statistics of switching can improve its long-term fitness, e.g., by adopting persister phenotypes with appropriate probability [7, 8]. The seemingly limitless ingenuity of evolutionary trial-and-error makes it plausible that virtually any statistical structure of the environment that remains constant over an evolutionary timescale could, in principle, be learnt by an evolving system, and harnessed to improve its fitness [9].

However, the statistical structure of the environment can itself change, and this change can be too quick to be learned by evolution. For example, an organism might experience a period of stability followed by a period of large fluctuations; or an environment where two resources are correlated, and then another where they are not. Note that our focus here is not the rapidity of fluctuations, but the slower timescale on which the *structure* of

those fluctuations changes. One expects such scenarios to be particularly common in an eco-evolutionary context. As an example, consider a bacterium in a small pool of water (Fig. 1A). Its immediate environment, shaped by local interactions, is fluctuating on the timescale at which the bacterium changes neighbors. The statistical properties of these fluctuations depend on the species composition of the pool. As such, the fast fluctuations are partially predictable, and learning their structure could help inform the fitness-optimizing strategy: a neighbor encountered in a recent past is likely to be seen in the near future. However, these statistics change on an ecological timescale, and such learning would therefore need to be accomplished by physiological, rather than evolutionary, mechanisms.

On a physiological timescale, this problem is highly nontrivial: the organism would have to perform inference from prior observations, encode them in memory, and act upon this knowledge (Fig. 1B). It is clear that solutions to this problem do exist: such behaviors, common in neural systems, can be implemented by neural-network-like architectures; and these known architectures can be translated into biochemical networks [10–14]. But single-celled organisms operate in a severely hardware-limited regime rarely probed by neuroscience. Streamlined by evolution, bacterial genomes quickly shed any unused complexity. Whether we could expect learning-like behaviors from bacteria depends on whether useful networks could be simple enough to plausibly be beneficial.

Known examples of phenotypic memory, e.g., when the response is mediated by a long-lived protein, can be interpreted as a simple form of learning [15, 16]; circuits capable of adapting to the current mean of a fluctuating signal, as in bacterial chemotaxis [17], also belong in this category. Prior theory work has also proposed

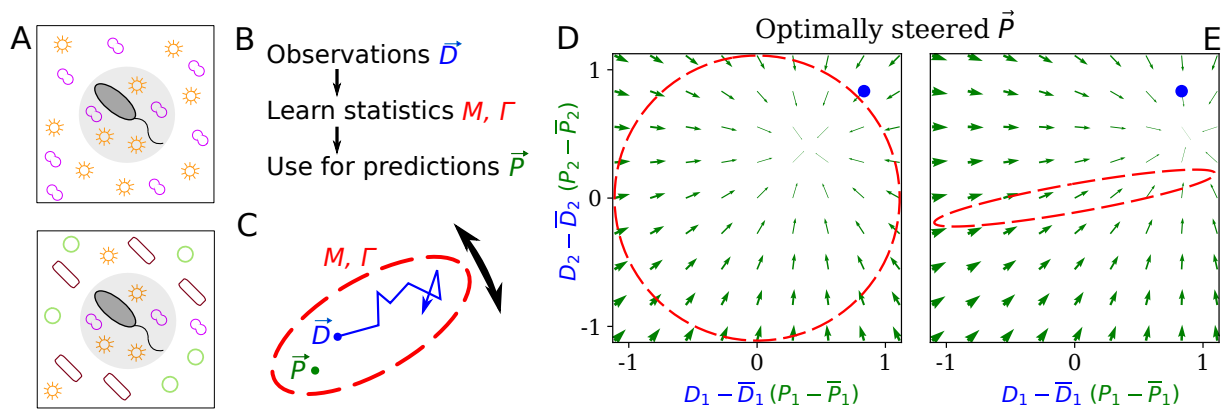


FIG. 1. Learning environment statistics can benefit living systems, but is a difficult problem. (A) An environment is characterized not only by its current state, but also by its *fluctuation structure*, which determines what changes are likely to occur in the future. In this cartoon, the immediate environment of a given bacterium (center) is shaped by its close neighbors, while the ensemble of likely future changes is determined by the species composition of the habitat. Two environments experienced as identical at a particular time could differ in the fluctuation structure; this difference can inform the fitness-maximizing strategy, but cannot be sensed directly. (B) Instead, the fluctuation structure would need to be learned from past observations, and used to inform future behavior. (C) To formalize the problem, we consider a situation where some internal physiological quantities $\vec{P}(t)$ must track fluctuating external factors $\vec{D}(t)$ undergoing a random walk. Since it is impossible to react instantaneously, \vec{P} always lags behind \vec{D} . The dashed ellipse illustrates the fluctuation structure of \vec{D} (encoded in parameters M and Γ , see text), and changes on a slower timescale than the fluctuations of \vec{D} . (D, E) The optimal behavior in the two-dimensional version of our problem, under a constrained maximal rate of change $\|\dot{P}\|^2$. For a given current \vec{D} (blue dot), the optimal control strategy would steer any current \vec{P} (green arrows) towards the best guess of the future \vec{D} , which depends on the fluctuation structure (red ellipse: (D) fluctuations are uncorrelated and isotropic; (E) fluctuations have a preferred direction). The optimal strategy is derived using control theory (SI section “Control theory calculation”).

that simple genetic circuits could learn more subtle binary features, such as a (transient) presence or absence of a correlation between two signals [18].

Here, we show that a simple generalization of a ubiquitous regulatory motif, the end-product inhibition, can learn, store, and “act upon” the information on continuous-valued features such as timescales and correlations of environmental fluctuations, and moreover, can do so near-optimally. We identify the key ingredients giving rise to this behavior, and argue that their applicability is likely more general than the simple metabolically-inspired example used here.

The setup

To model the general challenges of surviving in a fluctuating environment, consider a situation where some internal physiological quantities $\vec{P} = (P_1, \dots, P_N)$ must track fluctuating external variables $\vec{D} = (D_1, \dots, D_N)$. For example, the expression of a costly metabolic pathway would ideally track the availability of the relevant nutrient, or the solute concentration in the cytoplasm might track the osmolarity of the environment. In abstract terms, we describe these environmental pressures by the time-dependent $\vec{D}(t)$, and postulate that the organism fitness is determined by the average mismatch $-\sqrt{\langle \sum_{i=1}^N (P_i - D_i)^2 \rangle}$, a quantity we will henceforth call “performance”. Here and below, angular brackets denote

averaging over time.

If \vec{D} changes sufficiently slowly, the organism can sense it and adapt \vec{P} accordingly. We, instead, are interested in the regime of rapid fluctuations. When changes in \vec{D} are too rapid for the organism to match \vec{P} to \vec{D} exactly, it can rely on statistical structure. At the simplest level, the organism could match the mean, setting $\vec{P} \equiv \langle \vec{D} \rangle$. However, information on higher-order statistics, e.g. correlations between D_1 and D_2 , can further inform the behavior and improve fitness.

To see this, in what follows, we will consider the minimal case of such structured fluctuations, namely a N -dimensional vector $\vec{D} = (D_1, \dots, D_N)$ undergoing a random walk in a quadratic potential

$$\vec{D}(t + \Delta t) = \vec{D}(t) - M \cdot (\vec{D}(t) - \vec{\bar{D}}) \Delta t + \sqrt{2\Gamma\Delta t} \vec{\eta}, \quad (1)$$

with mean $\vec{\bar{D}}$, fluctuation strength Γ , independent Gaussian random variables $\vec{\eta}$ with zero mean and variance one, and the matrix M defining the potential.

In this system, the relevant “fluctuation structure” is determined by M and Γ . In one dimension, Eq. (1) gives D a variance of Γ/M . In two dimensions, denoting the eigenvalues of M as $\lambda_{1,2}$, the stationary distribution of the fluctuating \vec{D} is a Gaussian distribution with principal axes oriented along the eigenvectors of M , and standard deviations along these directions given by $\sqrt{\Gamma/\lambda_1}$ and $\sqrt{\Gamma/\lambda_2}$. Intuitively, we can think of the fluctuating \vec{D} as filling out an ellipse (Fig. 1C). Going forward,

when we refer to learning fluctuation structure, we mean learning properties of M and Γ .

If M and Γ are known, the optimal strategy minimizing $\langle (\vec{P} - \vec{D})^2 \rangle$, where $\vec{D}(t)$ is set by Eq. (1), can be computed exactly, as a function of the maximum allowed rate of change $\|\dot{P}\|^2$. (If we do not constrain $\|\dot{P}\|^2$, the optimal behavior is of course $\vec{P} = \vec{D}$.) Briefly, the optimal behavior is to steer \vec{P} towards the best guess of the expected future \vec{D} (see SI section ‘‘Control theory calculation’’). This best guess depends on the fluctuation structure, as illustrated by the comparison between Fig. 1D and 1E for an isotropic and an anisotropic M .

However, in our problem we will assume that M and Γ do not stay constant long enough to be learned by evolution, and thus are unknown to the system. In this regime, it is not clear that the behavior of an M - and Γ -optimized system is relevant. Nevertheless, we will describe a regulatory architecture consisting of common regulatory elements that will adapt its responsiveness to the fluctuation structure of its input (‘‘learn’’); for example, in the two-dimensional case, it will indeed develop the anisotropic response shown in Fig. 1E. Moreover, we will find the steady-state performance of our architecture to be near-optimal, when compared to the theoretical ceiling of a system that knows M and Γ perfectly.

Proposed architecture: end-product inhibition with an excess of regulators

The section above was intentionally very general. To discuss solutions available to cells, it is convenient to restrict the scope from this general formulation to a more specific metabolically-inspired case. From now onwards, let D_i be the instantaneous demand in metabolite x_i (determined by external factors), and P_i be the rate at which the metabolite is produced, both defined in units of metabolite concentration per unit time. The number of components of the vector \vec{D} now has the meaning of the number of metabolites, and we will denote it as N_x . The cell needs to match \vec{P} to \vec{D} (or, equivalently, maintain the homeostasis of the internal metabolite concentrations x_i).

The simplest way to solve this problem is via feedback inhibition. Consider first the case of a single metabolite x . If an accumulation of x inhibits its own synthesis, a decreased demand will automatically translate into a decreased production. For our purposes, we will model this scenario by placing the synthesis of metabolite x under the control of a regulator a (e.g., a transcription factor), which is, in turn, inhibited by x (Fig. 2A). For simplicity, we will measure regulator activity a directly in units of equivalent production of x . The dynamics of this system, linearized for small fluctuations of metabolite concentration x , can be written in the following form (see SI section

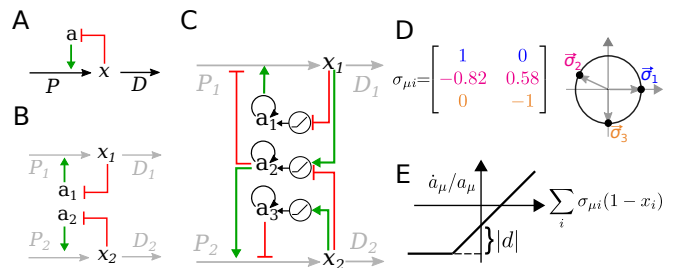


FIG. 2. The regulatory architecture we consider is a simple generalization of end-product inhibition. (A) Simple end-product inhibition (SEPI) for one metabolite. Green arrows show activation, red arrows inhibition. (B) Natural extension of SEPI to several metabolites. (C) We consider regulatory architectures with more regulators than metabolites, with added self-activation (circular arrows) and a nonlinear activation/repression of regulators a_μ by the metabolite concentrations x_i (pictograms in circles). (D) Visualizing a regulation matrix $\sigma_{\mu i}$ for two metabolites. In this example, the first regulator described by $\vec{\sigma}_1$ activates the production of x_1 ; the second inhibits x_1 and activates x_2 . For simplicity, we choose vectors of unit length, which can be represented by a dot on the unit circle. This provides a convenient way to visualize a given regulatory architecture. (E) The nonlinear dependence of regulator activity dynamics \dot{a}_μ/a_μ on metabolite concentrations x_i in our model (see Eq. (4)).

‘‘Simple end-product inhibition’’):

$$\dot{x} = P - D \frac{x}{x_0} \quad \text{source-sink dynamics of metabolite } x \quad (2a)$$

$$P = aP_0 \quad \text{definition of regulator activity } a \quad (2b)$$

$$\dot{a} = \frac{x_0 - x}{\lambda} \quad \text{regulator activity inhibited by } x \quad (2c)$$

Here, we introduced P_0 with dimension of production (concentration per time) to render a dimensionless. In Eq. (2c), λ has the units of concentration \times time, and setting $\lambda \equiv x_0 \tau_a$ defines a time scale for changes in regulator activity. Assuming the dynamics of metabolite concentrations x are faster than regulatory processes, and choosing the units so that $x_0 = 1$ and $P_0 = 1$, we simplify the equations to:

$$\begin{aligned} x &= P/D \\ P &= a \\ \tau_a \dot{a} &= 1 - x. \end{aligned} \quad (3)$$

We will refer to this architecture as simple end-product inhibition (SEPI). For two metabolites $\vec{x} = (x_1, x_2)$, the straightforward generalization is to have two independent copies of this circuit, with two regulators a_1, a_2 (Fig. 2B). Denoting the number of regulators as N_a , we note that in the SEPI architecture, there are as many regulators as there are metabolites: $N_a = N_x$.

The architecture we will describe builds on this widely used regulatory motif, and relies on three added ingredients:

1. an excess of regulators: $N_a > N_x$;

2. self-activation of regulators;
3. nonlinear activation/repression of the regulators a_μ by the metabolite concentrations x_i .

Here and below, we use index μ for regulators ($\mu = 1 \dots N_a$) and index i for metabolites ($i = 1 \dots N_x$).

These three ingredients, we claim, will be sufficient for the circuit to both learn higher order statistics and to use this information appropriately when matching the production to demand. It is important to emphasize that all three are readily accessible to cells. In fact, there are multiple ways to build regulatory circuits exhibiting the proposed behavior using common regulatory elements. To focus on the general mechanism rather than any one particular implementation, we will defer describing these example circuits until later in the text; here we will consider a minimal modification of Eq. (3) that contains the required ingredients:

$$x_i = P_i/D_i \quad (4a)$$

$$P_i = \sum_\mu \sigma_{\mu i} a_\mu \quad (4b)$$

$$\tau_a \dot{a}_\mu = a_\mu \max \left(d, \sum_i \sigma_{\mu i} (1 - x_i) \right) - \kappa a_\mu. \quad (4c)$$

This architecture arguably bears a similarity to neural networks, and, as we will see, the familiar intuition about the value of extra “hidden nodes” indeed holds. However, we caution the reader not to rely too heavily on this analogy. For example, here $\sigma_{\mu i}$ is a *constant* matrix describing how the activities of regulators a_μ control the synthesis of metabolites x_i .

For two metabolites ($N_x = 2$) as in Fig. 2C, each regulator is summarized by a 2-component vector $\vec{\sigma}_\mu = (\sigma_{\mu 1}, \sigma_{\mu 2})$; its components can be of either sign (or zero) and specify how strongly the regulator a_μ is activating or repressing the synthesis of metabolite x_i . For simplicity, below, we will choose these vectors to be of unit length. Then, each regulator $\vec{\sigma}_\mu$ is fully characterized by an angle in the (x_1, x_2) plane, which allows for a convenient visualization of the regulatory systems (Fig. 2D). The $\sigma_{\mu i}$ defines the regulatory logic of our system and does not change with time. The parameter $d \leq 0$ is included so we can tune the strength of the simple nonlinearity (Fig. 2E); below we set $d = 0$ (strong nonlinearity) unless explicitly stated otherwise. Finally, the parameter κ reflects degradation and is assumed to be small: $\kappa \ll x_0$. Previously, for SEPI, it could be neglected, but here, it will matter due to the nonlinearity; see SI section “Simple end-product inhibition” for more details. The parameters used in simulations are all listed in SI section “Parameters used in figures”.

Just like simple end-product inhibition in Eq. (3), the modified system Eq. (4) will correctly adapt production to any static demand (see SI section “Adaptation to static demand”). In the following, we will show that the added ingredients also enable learning the structure of fluctuating environments. For this purpose, we expose

our system to demands $D(t)$ with fixed means ($\overline{D}_i = 1$) but a changing fluctuation structure.

The regulatory architecture described above outperforms simple end-product inhibition by learning environment statistics

To show that our system is able to adapt to different fluctuation structures, we probe it with changing environmental statistics, and show that it, first, learns these statistics, and, second, is able to make use of this information in its behaviour.

For simplicity, we start with the 1-dimensional case (Fig. 3A-F). In dimension $N_x = 1$, an excess of regulators means we have both an activator a_+ and a repressor a_- for the production of x (Fig. 3A). This is reminiscent of paradoxical regulation [19]. We probe our system with changing environmental statistics by exposing it to a demand $D(t)$ with an increasing variance (Fig. 3B, C). As a reminder, here and below, the mean demand is fixed at 1.

Faced with a faster fluctuating input, our system up-regulates both a_+ and a_- while keeping $a_+ - a_-$ constant ($a_+ - a_- \approx \overline{D} = 1$; Fig. 3D). In this way, the two activity levels a_+ and a_- encode both the mean and the variance of fluctuations. Crucially, the system makes use of the information it stores: The increased regulator activities allow future changes in P to be faster. The system’s *responsiveness*, which we can define as $\mathcal{R} \equiv \frac{d\dot{P}}{dD}$, increases as $a_+ + a_-$ (Fig. 3E; see also SI section, “Defining the systems responsiveness”). As a result, as shown in Fig. 3F, our system is able to perform approximately equally well (after adaptation time) in each environment, unlike a system like simple end-product inhibition, which is unable to adapt its sensitivity. In summary, Figs. 3D-F show that the simple architecture of Fig. 3A can not only learn statistics of environment fluctuations, but also “act upon this knowledge,” effectively performing both computations of Fig. 1B.

The idea of learning the fluctuation structure is perhaps clearer in dimension $N_x = 2$, since the two demands can now be correlated with each other, and it seems intuitive that a system able to learn the typical direction of fluctuations (the angle α in Fig. 3H) should be able to track the input better. Indeed, as we saw in Figs. 1D-E, when environment fluctuations are anisotropic, the responsiveness of a well-adapted strategy must be anisotropic as well: the preferred direction must elicit a stronger response. Mathematically, the responsiveness \mathcal{R} is now a matrix $\mathcal{R}_{ij} = \frac{d\dot{P}_i}{dD_j}$, and for a well-adapted system we expect its eigenvectors to align with the principal directions of M . In Figs. 3G-L, Fig. 4 and Fig. 5A, our discussion will focus on this two-dimensional case.

Figs. 3G-L show the behavior of our system (Eq. (4)) with $N_a = 5$ regulators (Fig. 3G), exposed to an input

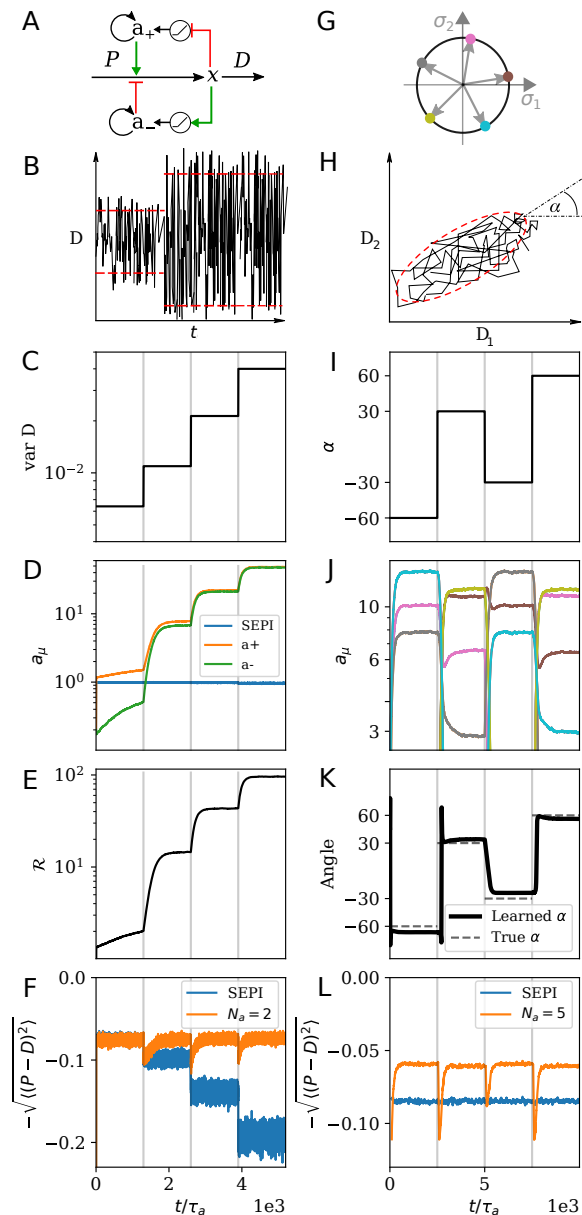


FIG. 3. The regulatory architecture we consider successfully learns environment statistics, and outperforms simple end-product inhibition. Left column in one dimension, right column in two. (A) Regulation of a single metabolite x with one activator a_+ and one repressor a_- . (B, C) The variance of D is increased step-wise (by increasing Γ). (D) Regulator activities a_{\pm} respond to the changing statistics of \vec{D} . For SEPI, the activity of its single regulator is unchanged. (E) Faced with larger fluctuations, our system becomes more responsive. (F) As fluctuations increase, SEPI performance drops, while the circuit of panel A retains its performance. Panels D-F show averages over 80 realizations. (G) In the 2d case, we consider a system with $N_a = 5$ regulators; visualization as in Fig. 2D. (H) Cartoon of correlated demands with a dominant fluctuation direction (angle α). (I) We use α to change the fluctuation structure of the input. (J) Regulator activities respond to the changing statistics of \vec{D} . Colors as in panel G. (K) The direction of largest responsiveness (“learned angle”; see text) tracks the α of the input. (L) The system able to learn the dominant direction of fluctuations outperforms the SEPI architecture, even if the timescale τ_a of SEPI is adjusted to match the faster responsiveness of the $N_a = 5$ system (see SI section “Parameters used in figures”). Panels J-L show averages over 40 realizations. Panels B and H are cartoons.

structured as shown in Fig. 3H, where we vary α (Fig. 3I). In other words, we rotate the fluctuation structure matrix M in Eq. (1), keeping its eigenvalues $\lambda_{1,2}$ fixed with $\sqrt{\lambda_1/\lambda_2} = 10$ (this fixes the ratio of major to minor semi-axis lengths).

With $N_a = 5$ regulators, matching the mean value of \vec{D} would leave $N_a - 2 = 3$ degrees of freedom that can be influenced by other parameters (such as variance in each dimension and correlation between different demands). And indeed, changing environment statistics induces strong changes in the regulator state adopted by the system (Fig. 3J). When viewed in the space of a_{μ} ’s, the pattern for how the stimulus parameters are mapped to the system’s internal state is not immediately discernible. However, this pattern becomes clear when we consider the responsiveness matrix \mathcal{R} . Fig. 3K plots the “learned angle”, defined as the direction of the dominant eigenvector of \mathcal{R} ; we find that it tracks the stimulus angle. Finally, Fig. 3L demonstrates that our architecture is able to make use of this learning, outperforming the SEPI system, whose responsiveness is isotropic and fixed.

The performance is near-optimal

In the previous section we have shown by example (Fig. 3) that the proposed regulatory architecture can learn statistics of the environment, and that this learning improves performance. We now characterize systematically the conditions under which learning improves performance and compare our system to the theoretical performance ceiling.

The fluctuation structure in our model is defined by Γ and M . We first investigate the dependence of performance on Γ (Fig. 4A), exposing our system to a two-dimensional input structured as in Fig 3H with $\sqrt{\lambda_1/\lambda_2} = 10$ as before, $\alpha = \pi/4$, and a changing Γ .

Although the input is two-dimensional, changing Γ scales the overall magnitude of fluctuations, and the behavior is analogous to the simpler one-dimensional example shown in the first column of Fig. 3. At $\Gamma = 0$ (static input), and by extension, for Γ finite but small, examining the steady state of Eq. (4) shows that only $N_x = 2$ out of N_a regulators can be active. In this regime, our system is essentially identical to SEPI—the extra regulators, though available, are inactive—and in fact performs slightly worse. This is because at nonzero κ , the steady state of Eq. (4) is slightly offset from the ideal state $\langle x_i \rangle = 1$. (While this effect can be corrected, it is only relevant in the parameter regime where no learning occurs, so we chose to keep Eq. (4) as simple as possible; for additional discussion, see SI section “Performance penalty from the degradation term”.)

When Γ becomes sufficiently large, the first term in Eq. (4c) (proportional to fluctuation size $\sqrt{\Gamma}$) for one of the inactive regulators finally exceeds, on average, the degradation term. At this point, the system enters the

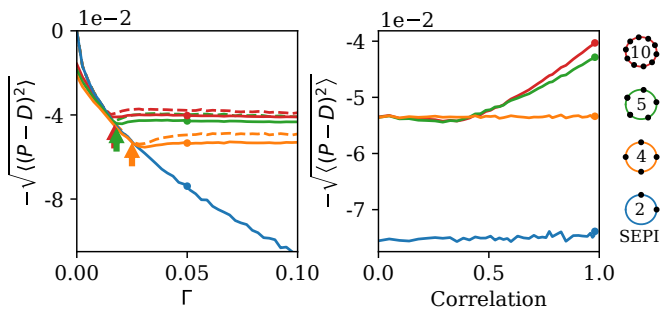


FIG. 4. The ability to learn statistics is most useful when fluctuations are large and/or strongly correlated. (A) The performance of different circuits shown as a function of Γ , which scales the fluctuation magnitude (input is two-dimensional and correlated, angle $\alpha = \pi/4$, anisotropy $\sqrt{\lambda_1/\lambda_2} = 10$). Once the fluctuations become large enough to activate the learning mechanism, performance stabilizes; in contrast, the SEPI performance continues to decline. Arrows indicate the theoretical prediction for the threshold value of Γ ; see SI section “The minimal Γ needed to initiate adaptation”. Dashed lines indicate the theoretical performance ceiling (calculated at equivalent Control Input Power, see text). (B) Comparison of circuit performance for inputs of the same variance, but different correlation strengths. $N_a = 4$ regulators arranged as shown can learn the variance but not correlation; the SEPI architecture is unable to adapt to either. Parameter Γ is held constant at 0.05; the marked points are identical to those highlighted in panel A (and correspond to fluctuation anisotropy $\sqrt{\lambda_1/\lambda_2} = 10$).

regime where the number of active regulators exceeds N_x , and its performance deviates from the SEPI curve. Beyond this point, further changes to the stimulus no longer affect performance, as our system is able to adapt its responsiveness to the changing fluctuation magnitude (compare to Fig. 3F). The threshold value of Γ satisfies $\sqrt{\Gamma} \propto \kappa$; the proportionality coefficient of order 1 depends on the specific arrangement of regulators but can be estimated analytically (see SI section “The minimal Γ needed to initiate adaptation”). The theoretically predicted deviation points are indicated with arrows, and are in agreement with the simulation results. When a regulator in the system is particularly well-aligned with the dominant direction of fluctuations, the deviation occurs sooner, explaining the better performance of our system when the regulators are more numerous.

To better assess the performance of our system, we compare it to the theoretical optimum derived from control theory, which we represent with dotted lines in Fig 4A. For given M and Γ , the family of optimal behaviors is parameterized by Control Input Power (CIP), defined as $\int \|\dot{P}\|^2 dt$. If \vec{P} could react infinitely fast, it would track \vec{D} perfectly, but maintaining such a perfect regulatory system would presumably be costly; constraining the CIP is thus a proxy for specifying the maximum tolerable cost. In order to compare our system with the optimal family of solutions, we compute $\frac{1}{T} \int_0^T \|\dot{P}\|^2 dt$ of our sys-

tem at each Γ (T is the simulation time), and compare to the performance of the optimally steered solution with a matched CIP; details of the calculation can be found in the SI section “Control theory calculation”. Fig. 4A demonstrates that the simple architecture we described not only benefits from matching its responsiveness to its input, but is in fact near-optimal when compared to *any* system of equivalent responsiveness.

Having investigated the effect of fluctuation variance (changing Γ), we turn to the effect of their correlation. Up to now, we subjected our system to a strongly correlated two-dimensional input with anisotropy $\sqrt{\lambda_1/\lambda_2} = 10$ (illustrated, to scale, in Fig. 1E). We will now consider a range of anisotropy values, down to anisotropy 1 (uncorrelated fluctuations, Fig. 1D), keeping the variances of D_1 and D_2 constant, $\alpha = \pi/4$ as before, and $\Gamma = 0.05$.

The result is presented in Fig. 4B. With $N_a = 5$ or larger, our system is able to take advantage of the correlation, assuming it is strong enough to activate the learning mechanism. (In fact, its performance can reach values that exceed the theoretical ceiling achievable by any system that assumes the two dimensions of \vec{D} to be independent, and thus *must* be exploiting the correlation in its inputs; see SI section “The system makes use of correlations in the input” and Fig. S1.) For $N_a = 4$, the performance curve remains flat. This is because the four regulators are arranged as two independent copies of the system shown in Fig. 3A (one $\{a_+, a_-\}$ pair for each of the two inputs); this architecture can take advantage of the learned variance, but not the correlation. Finally, the SEPI architecture can adapt to neither variance nor correlation; its performance curve is also flat, but is lower. As expected, the advantage of our architecture manifests itself in environments with periods of large and/or strongly correlated fluctuations.

The behavior is generalizable

The model described above was a proof of principle, showing that simple regulatory circuits could learn the fluctuation structure of their inputs. Given the simplicity of our model, it is not to be expected that the exact dynamics of Eq. (4) are replicated in real cells. However, the benefit of this simplicity is that we can now trace this behavior to its key ingredients, which we expect to be more general than the model itself.

Specifically in the context of our model, we described our three ingredients as an excess of regulators, nonlinearity, and self-activation. The role of the first two is examined in detail in Fig. 5A (for the two-dimensional case); self-activation is discussed in the SI section “The role of self-activation”. In Fig. 5A, the parameter d on the horizontal axis is the strength of nonlinearity (see Fig. 2E), from perfectly linear at $d = -\infty$, to strongly nonlinear at $d = 0$. The vertical axis corresponds to an increasing number of regulators N_a , which we label as in Fig. 2D. The point approximately corresponding to

the SEPI architecture is highlighted (a linear system of $N_a = N_x = 2$ activators).¹ We see that in the nonlinear regime, adding regulators improves performance; note, however, that even a single extra regulator ($N_a = 3$) already provides a significant benefit over the SEPI architecture. For completeness, we also include the simplest system with a single regulator co-activating both x_1 and x_2 (bottom row of Fig. 5A).

Fig. 5A shows that the reported behavior requires N_a to exceed N_x , and d to be sufficiently large. However, these ingredients are more general than the specific implementation in Eq. (4). In our model, additional regulators were required because they supplied the slow degrees of freedom to serve as memory; such degrees of freedom could be implemented in other ways, for example, as phosphorylation or methylation [17]. Similarly, while nonlinearity is essential (linear dynamics cannot couple to higher-order terms, such as fluctuation magnitude), its exact functional form may be changed while retaining the learning behavior (see SI section “Nonlinearity as a sensor of fluctuation variance”). Finally, the explicitly self-catalytic behavior of a_μ in our model is only one possible strategy for translating the stored memory into a faster response; as an example, in Fig. 3A the regulators a_+ and a_- could activate each other rather than themselves.

To demonstrate the broader generality of these ingredients, we constructed two circuits with very different architectures, both reproducing the results of Fig. 3C-F. One of these, based on a pair of allosteric enzymes, and with the toy nonlinearity of Fig. 2E replaced by more realistic cooperative binding, implements dynamics similar to those considered above and is discussed in the SI (see Fig. S3).

The other circuit is different not only in appearance, but also in dynamics, and is shown in Fig. 5B. Here, instead of seeking to match P to D , we seek to maintain the homeostasis of x perturbed by external factors. (Previously, the two formulations were equivalent; for greater generality, in Fig. 5B we focus on the latter.) In this implementation, the production and degradation of x are both catalyzed by a single bifunctional enzyme. Despite looking quite different from Fig. 3A, this architecture possesses the same key ingredients, and can exhibit the same learning behavior (see Fig. S5). Briefly, the responsiveness of this circuit scales with the overall expression of the enzyme E , and larger fluctuations of x lead to up-regulation of E due to the nonlinearity, as before. For more details, see SI section “Realistic biochemical implementations”.

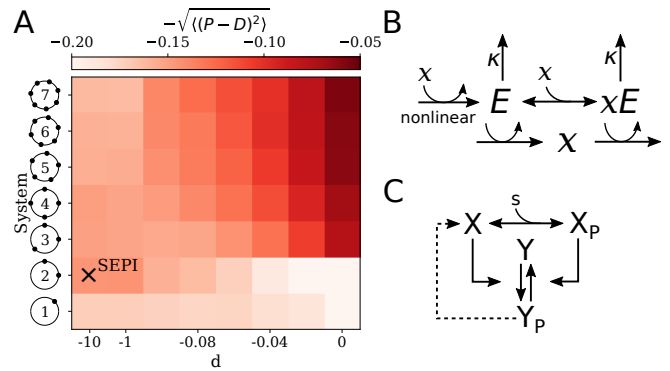


FIG. 5. Two key ingredients enabling learning are nonlinearity and an excess of regulators. (A) System performance in the two-dimensional case $N_x = 2$, shown as a function of the number of regulators N_a (vertical axis) and the strength of nonlinearity d (horizontal axis; $d = -10$ is indistinguishable from a linear system with $d = -\infty$). The SEPI-like architecture (linear with $N_a = 2$; see text) is highlighted. Each data point is averaged over α (see Fig 3H). (B) An alternative circuit capable of learning fluctuation variance to better maintain homeostasis of a quantity x . Synthesis and degradation of x are catalyzed by the same bifunctional enzyme, whose production is regulated nonlinearly by x itself. For more details see the SI section “Realistic biochemical implementations”. (C) Solid arrows: a common two-component architecture of bacterial sensory systems with a bifunctional histidine kinase (X) and its cognate response regulator (Y). Adding an extra regulatory link (nonlinear auto-amplification, dashed arrow) can endow this system with self-tuned reactivity learning the statistics of the input; see text.

Interestingly, the same logic can be implemented as a small modification of the standard two-component signaling architecture (Fig. 5C). In this architecture, the signal s determines the concentration of the phosphorylated form Y_P of the response regulator Y ; the rapidity of the response is determined by the expression of the histidine kinase X , present at a much lower copy number.² Thus, much like in Fig. 5B, a nonlinear activation of X by Y_P (known as autoregulation [21] or autoamplification [16], and shown as a dashed arrow in Fig. 5C) would endow this signaling system with self-tuned reactivity that learns the statistics of the input.

Discussion

In this paper we have studied a regulatory architecture which is able to infer higher order statistics from fluctuating environments and use this information to in-

¹ The correspondence between the labeled point and the SEPI architecture is only approximate, because all models represented in Fig. 5A include self-activation and a small degradation term, while the SEPI architecture does not. However, with only 2 regulators, neither difference has a significant performance effect (see SI section “The role of self-activation”).

² Although the signaling architecture of Fig. 5C, at least in some parameter regimes, is known to be robust to the overall concentrations of X and Y [20], this robustness property applies only to the steady-state mapping from s to Y_P , not the kinetics.

form behavior. For concreteness, we phrased the regulatory task as seeking to match the production \bar{P} of one or two metabolites to a rapidly fluctuating demand \bar{D} . Alternatively, and perhaps more generally, the circuits we constructed can be seen as maintaining the homeostasis in a quantity \bar{x} that is continually perturbed by external factors. We demonstrated that a simple architecture was capable of learning the statistics of fluctuations of its inputs and successfully using this information to optimize its performance. We considered one-dimensional and two-dimensional examples of such behavior.

In one dimension, learning the statistics of the input meant our circuit exhibited a self-tuned reactivity, learning to become more responsive during periods of larger fluctuations. Importantly, we have shown that this behavior can be achieved by circuits that are highly similar to known motifs, such as feedback inhibition (Fig. 2A, C) or two-component signaling (Fig. 5B, C). The latter connection is especially interesting: There are at least a few examples of two-component systems where autoamplification, a necessary ingredient for the learning behavior discussed here, has been reported [22, 23]. Moreover, in the case of the PhoR/PhoB two-component system in *E. coli*, such autoamplification has been experimentally observed to allow cells to retain memory of a previously experienced signal (phosphate limitation) [16], a behavior the authors described as learning-like. As reported, this behavior constitutes a response to the signal mean and is similar to other examples of simple phenotypic memory (e.g. [15]); however, our analysis demonstrates that a similar architecture may also be able to learn more complex features. Such a capability would be most useful in contexts where the timescale of sensing could plausibly be the performance bottleneck. Since transcriptional

processes are generally slower than the two-component kinetics, we expect our discussion to be more relevant for two-component systems with non-transcriptional read-out, such as those involved in chemotaxis or efflux pump regulation.

In the two-dimensional case, our simple circuit was able to learn and unlearn transient correlation structures of its inputs. Our argument was a proof of principle that, e.g., the gut bacteria could have the means to not only sense, but also predict nutrient availability based on correlations learned from the past, including correlations that change over faster-than-evolutionary timescales, such as the life cycle (or dietary preferences) of the host. Importantly, we showed that this ability could come cheaply, requiring only a few ingredients beyond simple end-product inhibition.

The mechanism described here could suggest new hypotheses for the functional role of systems with an excess of regulators, as well as new hypotheses for bacterial function in environments with changing structure.

Python scripts reproducing all figures are available upon request and will be published alongside the final version of the manuscript.

Acknowledgments

We thank M. Goulian, A. Murugan, and B. Weiner for helpful discussions. SL was supported by the German Science Foundation under project EN 278/10-1; CMH was supported by the National Science Foundation, through the Center for the Physics of Biological Function (PHY-1734030) and the Graduate Research Fellowship Program.

-
- [1] D. Bell-Pedersen, V. M. Cassone, D. J. Earnest, S. S. Golden, P. E. Hardin, T. L. Thomas, and M. J. Zoran, Circadian rhythms from multiple oscillators: lessons from diverse organisms, *Nature Reviews Genetics* **6**, 544 (2005).
 - [2] K. Husain, W. Pittayakanchit, G. Pattanayak, M. J. Rust, and A. Murugan, Kalman-like self-tuned sensitivity in biophysical sensing, *Cell Systems* **9**, 459 (2019).
 - [3] M. A. Savageau, Escherichia coli habitats, cell types, and molecular mechanisms of gene control, *The American Naturalist* **122**, 732 (1983).
 - [4] I. Tagkopoulos, Y.-C. Liu, and S. Tavazoie, Predictive behavior within microbial genetic networks, *Science* **320**, 1313 (2008).
 - [5] A. Mitchell, G. H. Romano, B. Groisman, A. Yona, E. Dekel, M. Kupiec, O. Dahan, and Y. Pilpel, Adaptive prediction of environmental changes by microorganisms, *Nature* **460**, 220 (2009).
 - [6] A. Mitchell and W. Lim, Cellular perception and misperception: Internal models for decision-making shaped by evolutionary experience, *BioEssays* **38**, 845 (2016).
 - [7] E. Kussell and S. Leibler, Phenotypic diversity, population growth, and information in fluctuating environments, *Science* **309**, 2075 (2005).
 - [8] J.-W. Veening, W. K. Smits, and O. P. Kuipers, Bistability, epigenetics, and bet-hedging in bacteria, *Annu. Rev. Microbiol.* **62**, 193 (2008).
 - [9] R. A. Watson and E. Szathmary, How can evolution learn?, *Trends in ecology & evolution* **31**, 147 (2016).
 - [10] A. Hjelmfelt, E. D. Weinberger, and J. Ross, Chemical implementation of neural networks and turing machines, *Proceedings of the National Academy of Sciences* **88**, 10983 (1991).
 - [11] T. J. Kobayashi, Implementation of dynamic Bayesian decision making by intracellular kinetics, *Physical Review Letters* **104**, 228104 (2010).
 - [12] F. Fages, G. Le Guludec, O. Bournez, and A. Pouly, Strong turing completeness of continuous chemical reaction networks and compilation of mixed analog-digital programs, in *International conference on computational methods in systems biology* (Springer, 2017) pp. 108–127.
 - [13] Y. Katz and M. Springer, Probabilistic adaptation in changing microbial environments, *PeerJ* **4**, e2716 (2016).
 - [14] Y. Katz, M. Springer, and W. Fontana, Embody-

- ing probabilistic inference in biochemical circuits, arXiv:1806.10161.
- [15] G. Lambert and E. Kussell, Memory and fitness optimization of bacteria under fluctuating environments, *PLoS Genet* **10**, e1004556 (2014).
- [16] S. M. Hoffer, H. V. Westerhoff, K. J. Hellingwerf, P. W. Postma, and J. Tommassen, Autoamplification of a Two-Component Regulatory System Results in “Learning” Behavior, *Journal of Bacteriology* **183**, 4914 (2001).
- [17] N. Barkai and S. Leibler, Robustness in simple biochemical networks, *Nature* **387**, 913 (1997).
- [18] M. Sorek, N. Q. Balaban, and Y. Loewenstein, Stochasticity, bistability and the wisdom of crowds: a model for associative learning in genetic regulatory networks, *PLoS Comput Biol* **9**, e1003179 (2013).
- [19] Y. Hart, Y. E. Antebi, A. E. Mayo, N. Friedman, and U. Alon, Design principles of cell circuits with paradoxical components, *Proceedings of the National Academy of Sciences* **109**, 8346 (2012).
- [20] E. Batchelor and M. Goulian, Robustness and the cycle of phosphorylation and dephosphorylation in a two-component regulatory system, *Proceedings of the National Academy of Sciences* **100**, 691 (2003).
- [21] M. Goulian, Two-component signaling circuit structure and properties, *Current opinion in microbiology* **13**, 184 (2010).
- [22] D. Shin, E.-J. Lee, H. Huang, and E. A. Groisman, A positive feedback loop promotes transcription surge that jump-starts *Salmonella* virulence circuit, *Science* **314**, 1607 (2006).
- [23] C. L. Williams and P. A. Cotter, Autoregulation is essential for precise temporal and steady-state regulation by the *Bordetella* BvgAS phosphorelay, *Journal of Bacteriology* **189**, 1974 (2007).

Supplementary material

S1 Simple end-product inhibition

As the starting point of our regulatory architecture we consider a basic form of end-product inhibition (SEPI). The environment is modeled by a time-dependent (externally induced) demand $D(t)$ for metabolite x which is produced at a rate P (controlled by the system); both D and P are defined in units of metabolite concentration per unit time. The depletion of the metabolite depends on its concentration x and the demand D . Assuming first-order kinetics (or, alternatively, expanding a general function to linear order in small fluctuations of x) the dynamics of x is:

$$\dot{x} = P - D \frac{x}{x_0}. \quad (\text{S1})$$

Further, we consider the temporal evolution of the regulator activity a

$$\dot{a} = h(x, a). \quad (\text{S2})$$

By linearizing $h(x, a)$ around the stationary values (x_0, a_0) we get

$$\dot{a} = \lambda_x(x_0 - x) + \lambda_a(a_0 - a). \quad (\text{S3})$$

To examine this equation we introduce the Fourier transforms $\tilde{a}(\omega) = \mathcal{F}[a(t) - a_0]$ and $\tilde{x}(\omega) = \mathcal{F}[x(t) - x_0]$ and get

$$i\omega\tilde{a} = -\lambda_x\tilde{x} - \lambda_a\tilde{a} \quad \Rightarrow \quad \tilde{a}(\omega) = -\frac{\lambda_x\tilde{x}(\omega)(\lambda_a - i\omega)}{\lambda_a^2 + \omega^2}. \quad (\text{S4})$$

Equation (S4) shows that if the support of $\tilde{x}(\omega)$ is restricted to high frequencies, $\omega \gg \lambda_a$, then the degradation term $\lambda_a(a_0 - a)$ in Eq. (S3) is negligible. Including it would only add a restoring force, reducing the amplitude of fluctuations of a , and decreasing the performance of the system. Since we are interested in the regime of fast fluctuations of x we choose to omit this term in the SEPI system. With $\lambda_x = 1/\lambda$ we arrive at the dynamics used in the main text:

$$\begin{cases} \dot{x} = P - D \frac{x}{x_0} & \text{source-sink dynamics of metabolite } x \\ P = aP_0 & \text{definition of regulator activity } a \\ \dot{a} = \frac{x_0 - x}{\lambda} & \text{regulator activity inhibited by } x \end{cases}$$

In the nonlinear system (Eq. (3) of the main text), however, fast fluctuations of x can cause the growth of a (as discussed in the section ‘‘The nonlinearity as a sensor of the fluctuation variance’’), thereby inducing slow frequency modes to its dynamics. Thus, in the nonlinear case, we cannot omit the degradation term.

S2 Performance penalty from the degradation term

The model considered in the main text modifies the SEPI architecture as follows:

$$x_i = P_i/D_i \quad (\text{S5})$$

$$P_i = \sum_{\mu} \sigma_{\mu i} a_{\mu} \quad (\text{S6})$$

$$\tau_a \dot{a}_{\mu} = a_{\mu} \max \left(d, \sum_i \sigma_{\mu i} (x_0 - x_i) \right) - \kappa a_{\mu}. \quad (\text{S7})$$

Consider the case of a static input. We observe that if x_0 is set to 1, as in the main text, the presence of the degradation term causes the equilibrium point of these dynamics to be displaced away from $x_i = 1$. Therefore, for a static input, the performance of this system—the degree of mismatch between P_i and D_i , or, equivalently, the deviation of x_i from 1—is actually worse than the performance of the original SEPI.

While the case of a static input is irrelevant for the discussion in the main text, this slight offset leads to a performance penalty also for a fluctuating input. Indeed, time-averaging Eq. (S7) shows that for any active regulator, we must have

$$\left\langle f \left(\sum_i \sigma_{\mu i} (1 - x_i) \right) \right\rangle = \kappa, \quad (\text{S8})$$

where f is the nonlinearity in our equation, $f(\gamma) = \max(d, \gamma)$. Clearly, we will in general again have $\langle x_i \rangle \neq 1$; this is particularly obvious in the limit of small fluctuations when the nonlinearity is “not active”, such that $f(\gamma) = \gamma$.

This effect could be corrected by shifting x_0 . In the interest of keeping our model as close to SEPI as possible, we chose not to do so: this penalty is only significant in the regime where no learning occurs, and is otherwise outweighed by the performance increase due to self-tuned responsiveness, with the additional benefit of simplifying the discussion in the main text. Even if optimizing x_0 could make the performance slightly closer to the optimal bound, this kind of fine-tuning seems irrelevant in a biological context.

S3 Defining the systems responsiveness

In the main text we use a measure for the “responsiveness” of our system to changes in the demand $D(t)$. In this section it is shown in detail how this measure is defined. The central aim of the considered regulatory model is to match the time-dependent demand \vec{D} with the regulated production \vec{P} . The temporal evolution of \vec{P} is given by:

$$\dot{P}_i = \sum_{\mu} \sigma_{i\mu} \dot{a}_{\mu}, \quad (\text{S9})$$

with

$$\tau_a \dot{a}_{\mu} = a_{\mu} \max \left(d, \sum_i \sigma_{\mu i} (1 - P_i / D_i) \right) - \kappa a_{\mu}. \quad (\text{S10})$$

For a static demand $D_i = 1$ the production relaxes to a constant value $P_i \approx 1$ (where we assumed small κ) and consequently $\dot{P}_i = 0$. A deviation δD_i from the static demand will lead to a change of the production P_i - the larger \dot{P}_i , the faster the response to the changed demand. Therefore, we define the responsiveness of the production P_i to the demand D_j as $\mathcal{R}_{ij} = \frac{d\dot{P}_i}{dD_j}$. When assuming small fluctuations the explicit expression for the responsiveness is then given by:

$$\frac{d\dot{P}_i}{dD_j} = \sum_{\mu} \sigma_{i\mu} \frac{d\dot{a}_{\mu}}{dD_j} \approx \sum_{\mu} \sigma_{i\mu} a_{\mu} \sigma_{\mu j} \frac{P_i}{D_j^2} \approx \sum_{\mu} \sigma_{i\mu} a_{\mu} \sigma_{\mu j}. \quad (\text{S11})$$

As an example we consider the one-dimensional system studied in Fig. 3 A-F in the main text for which the responsiveness is

$$\mathcal{R} = \frac{d\dot{P}}{dD} = \sigma_{1+} a_+ \sigma_{+1} + \sigma_{1-} a_- \sigma_{-1} = a_+ + a_-, \quad (\text{S12})$$

where we used that $\sigma_{1+} = 1$ and $\sigma_{1-} = -1$.

S4 Control theory calculation

The problem we set is minimizing $\langle (\vec{P} - \vec{D})^2 \rangle$, where \vec{D} follows the dynamics of Eq. (1) in the main text,

$$\vec{D}(t + \Delta t) = \vec{D}(t) + M \cdot \left(\vec{\bar{D}} - \vec{D}(t) \right) \Delta t + \sqrt{2\Gamma\Delta t} \vec{\eta}. \quad (\text{S13})$$

We then wish to calculate the optimal way of steering \vec{P} . For simplicity, we will set the mean $\vec{\bar{D}} = 0$ (in the context of this abstract problem, this is equivalent to working with mean-shifted variables $\delta \vec{D} \equiv \vec{D} - \vec{\bar{D}}$ and similarly $\delta \vec{P} \equiv \vec{P} - \vec{\bar{D}}$). We can start by discretizing the above equation,

$$D_{t+1} = D_t - \tilde{M} D_t + \xi_t, \quad (\text{S14})$$

where $\tilde{M} \equiv M\Delta t$, and ξ has variance $2\Gamma\Delta t$. We seek to determine the optimal way to steer P ; in other words, the function $\phi_t(P_t, D_t)$ (“control policy”) dictating how P should be changed in a given time step:

$$P_{t+1} = P_t + u_t \quad (\text{S15})$$

$$u_t = \phi_t(P_t, D_t). \quad (\text{S16})$$

We then can define our cost function, which combines a cost for the magnitude of u_t (how quickly we can change \vec{P}), and the difference between \vec{P} and \vec{D} :

$$\text{Cost} = \mathbb{E} \left(\rho \sum_{\tau=0}^{N-1} \|u_\tau\|^2 + \sum_{\tau=0}^N \|P_\tau - D_\tau\|^2 \right). \quad (\text{S17})$$

The $\phi(P_t, D_t)$ describing the optimal behavior is the one that minimizes this cost. In order to solve for $\phi(P_t, D_t)$, we follow standard control theory techniques and define the “cost-to-go” function,

$$V_t(p_t, d_t) = \min_{\phi_t \dots \phi_{N-1}} \mathbb{E} \left[\left(\rho \sum_{\tau=t}^{N-1} \|u_\tau\|^2 + \sum_{\tau=t}^N \|P_\tau - D_\tau\|^2 \right) \begin{array}{l} P_t = p_t, D_t = d_t \\ D_{\tau+1} = (\mathbf{1} - \tilde{M})D_\tau + \xi_\tau \\ P_{\tau+1} = P_\tau + u_\tau \\ u_\tau = \phi_\tau(P_\tau, D_\tau) \end{array} \right]. \quad (\text{S18})$$

This function defines the smallest cost of all remaining steps; in particular, the total cost that we are trying to minimize is $V_0(0, 0)$. The cost-to-go satisfies the boundary condition

$$V_N(p, d) = \|p - d\|^2 \quad (\text{S19})$$

and the following recursive relation:

$$V_t(p, d) = (p - d)^2 + \min_v \left\{ \rho \|v\|^2 + \mathbb{E}_\xi V_{t+1}(p + v, (1 - \tilde{M})d + \xi) \right\}. \quad (\text{S20})$$

Since our system is Gaussian, this recursive relation can be solved by adopting a quadratic ansatz:

$$V_t(p, d) = p^\top A_t p - 2d^\top B_t p + d^\top C_t d + Q_t, \quad (\text{S21})$$

Solving for the matrices A_t , B_t , C_t , and Q_t , gives us the following recursive relations:

$$\begin{cases} Q_t = Q_{t+1} + 2\Gamma \Delta t \text{tr} C_{t+1} \\ A_t = \mathbf{1} + \rho A_{t+1} (\rho + A_{t+1})^{-1} \\ B_t = \mathbf{1} + \rho (\mathbf{1} - \tilde{M}) B_{t+1} (\rho + A_{t+1})^{-1} \\ C_t = \mathbf{1} + (\mathbf{1} - \tilde{M}) [C_{t+1} - B_{t+1} (\rho + A_{t+1})^{-1} B_{t+1}^\top] (\mathbf{1} - \tilde{M}) \end{cases} \quad (\text{S22})$$

Since our problem is to minimize the cost at steady state (known in control theory as an “infinite horizon” problem, $N \mapsto \infty$), we are interested in the fixed point of this mapping, specifically the matrices A_∞ , B_∞ to which this mapping converges when we start from $A_N = B_N = C_N = \mathbf{1}$ and $Q_N = 0$ (as defined by Eq. (S19)).

Since A_N is the identity matrix, all A_t are proportional to the identity matrix as well: $A_t = \alpha_t \mathbf{1}$, where $\alpha_t = 1 + \frac{\rho \alpha_{t+1}}{\rho + \alpha_{t+1}}$. The fixed point of this mapping is $\alpha = \frac{1 + \sqrt{1 + 4\rho}}{2} \geq 1$. Similarly, the fixed point of B_t is $B = [\mathbf{1} - \frac{\rho}{\rho + \alpha} (\mathbf{1} - \tilde{M})]^{-1}$. Expressing this in terms of α only:

$$B = \alpha [\mathbf{1} + (\alpha - 1) \tilde{M}]^{-1}$$

With these expressions, the optimal “control policy” is defined by the value of v that minimizes Eq. S20. This defines the optimal way to change \vec{P} for a given observed \vec{D} :

$$u = \frac{1}{\alpha} \left([\mathbf{1} + (\alpha - 1) \tilde{M}]^{-1} (\mathbf{1} - \tilde{M}) \vec{D} - \vec{P} \right), \quad (\text{S23})$$

or, restoring the notations of the main text, including a non-zero \vec{D} :

$$u = \frac{1}{\alpha} \left([\mathbf{1} + (\alpha - 1) M \Delta t]^{-1} (\mathbf{1} - M \Delta t) (\vec{D} - \vec{D}) - \vec{P} \right), \quad (\text{S24})$$

This u is the *exact* solution to the discrete version of the problem we considered. Since our simulations in this work use a discrete timestep, this is the form we use. Nevertheless, it is instructive to consider the small- Δt , large-CIP limit such that Δt and $(\alpha - 1)\Delta t$ are both small compared to inverse eigenvalues of M . In this case we have, to first order in Δt :

$$u = \frac{1}{\alpha} \left([\mathbb{1} - \alpha M \Delta t] (\vec{D} - \vec{D}) - \vec{P} \right).$$

This leads to the following, and very intuitive, form of the optimal control dynamics:

$$\begin{aligned} \vec{D} &\mapsto \vec{D} - M \Delta t (\vec{D} - \vec{D}) + \xi, \\ \vec{P} &\mapsto \vec{P} - M \Delta t (\vec{D} - \vec{D}) + \frac{1}{\alpha} ((\vec{D} - \vec{D}) - \vec{P}). \end{aligned} \tag{S25}$$

In other words, at every step the change in \vec{P} mirrors the average expected change in \vec{D} , with an extra term seeking to reduce their deviation. Note also that setting $\alpha = 1$ (infinite CIP) corresponds to steering \vec{P} directly to the expected value of \vec{D} at the next timestep, as expected.

S5 The system makes use of correlations in the input

Fig. 4B in the main text demonstrated that, as the fluctuating inputs become increasingly correlated, our architecture is able to outperform SEPI by an increasingly wide margin. The natural interpretation of this result is that the system is able to learn and exploit this correlation. Technically, however, one might note that this observation alone does not yet prove that our architecture is able to appropriately use the information it learned about specifically *correlation*. For example, it could be that strongly correlated inputs are somehow inducing a stronger increase in reactivity, causing the system to be generally faster, but without benefiting specifically from the correlated nature of its inputs.

Rather than focusing on excluding this specific scenario (which could be done by comparing the CIP values along the curves shown in Fig. 4B), we will show that with a sufficient number of regulators, our architecture can perform better than the theoretical ceiling achievable by *any* strategy that assumes the inputs to be independent. This will formally prove that, at least for some parameters, our system's improved performance must necessarily make use of the correlation of its inputs. Although the argument is somewhat academic in nature (we will prove our point using $N_a = 25$ regulators), it is theoretically pleasing, and so we present it here.

Specifically, we consider a system subjected to inputs structured as shown in Fig. 3H, with angle $\alpha = \pi/4$ so that the two inputs have the same variance. Fig. S1 shows the performance of our architecture for several values of the number of regulators N_a , plotted as curves parameterized by the degradation rate κ . The degradation rate controls how large the a_μ can become: a high value of κ leads to lower average steady-state values of the regulator activities, causing the system to be less responsive to changes in D . Thus, κ can be used to set the CIP of the regulatory system, allowing us to plot these performance curves in the “performance vs. CIP” axes traditional for control theory.

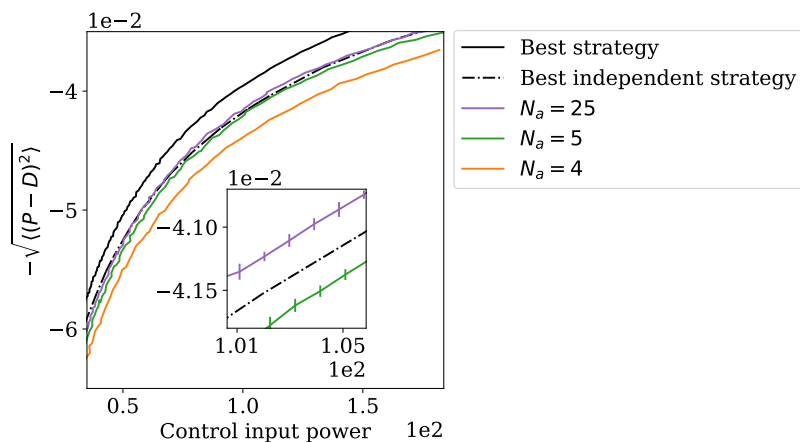


FIG. S1. The adapting system can perform better than the best independence-assuming strategy.

Reassuringly, all these performance curves are located below the optimal control-theory ceiling computed for the true correlation structure of the input. However, the plot also shows the “best independent” curve, defined as follows. Consider all possible matrices M corresponding to uncorrelated inputs: $M = \begin{pmatrix} \lambda_1 & 0 \\ 0 & \lambda_2 \end{pmatrix}$. Each such M defines a family of control strategies (that would have been optimal if this M were the true M governing the dynamics of the input); this family is indexed by a parameter ρ as described above. A system following an (independence-assuming) strategy $M = \begin{pmatrix} \lambda_1 & 0 \\ 0 & \lambda_2 \end{pmatrix}$ while faced with the actual (partially correlated) inputs will exhibit a certain performance $\mathcal{P}(\lambda_1, \lambda_2, \rho)$ and a certain CIP, which we denote $\text{CIP}(\lambda_1, \lambda_2, \rho)$. With these notations, the “best independent” curve is defined as

$$\mathcal{P}(\text{CIP} = \chi) = \max_{\lambda_1, \lambda_2} \{ \mathcal{P}(\lambda_1, \lambda_2, \rho) \text{ for } \rho \text{ such that } \text{CIP}(\lambda_1, \lambda_2, \rho) = \chi \}$$

We note that the correlated-input CIP is different from the independent-input CIP that a given strategy would have incurred if faced by the input for which it is optimal. In particular, while the latter can be computed analytically, the former has to be evaluated in simulations. This makes the optimization procedure computationally costly; thankfully, the symmetry ensured by choosing $\alpha = \pi/4$ allows restricting the search to isotropic strategies $M = \begin{pmatrix} \lambda & 0 \\ 0 & \lambda \end{pmatrix}$, reducing the problem dimensionality from three parameters $\{\lambda_1, \lambda_2, \rho\}$ to more manageable two $\{\lambda, \rho\}$.

The result is shown in Fig. S1 as a dashed line. As highlighted in the inset, with enough regulators, our architecture is indeed able to outperform the theoretical ceiling of the best independence-assuming strategy. Although $N = 25$ regulators is of course a regime irrelevant for biological applications, the aim of this argument was to formally prove a theoretical point, namely that the system as constructed must necessarily be making use of the correlation in the input signal, at least for some values of the parameters; by construction, the “best independent” curve is a high bar to clear.

S6 Nonlinearity as a sensor of fluctuation variance

In the main text we argue that the nonlinearity in the dynamics of the regulator concentrations acts as a sensor for the variance of the fluctuations. To see this, we consider the dynamics of one regulator that is controlling the production of one metabolite:

$$\tau_a \dot{a} = a \max(d, 1 - P/D) - \kappa a. \quad (\text{S26})$$

To simplify notation we define $\gamma := 1 - P/D$. Since the dynamics of a are slow compared to D , the fluctuations of γ are on a faster timescale than the regulator dynamics. If the fluctuations of γ are small, the nonlinearity in the max function is “not activated”: $\max(d, \gamma) = \gamma$. In this case, the temporal average of $\max(d, \gamma)$ is zero. In contrast, if the fluctuations are strong enough, the nonlinearity is activated (see Fig. S2). Then, the temporal average is positive, leading to an additional growth of a . Due to the resulting larger values of a , the response of the system becomes faster, making the match between P and D better and thus serving to decrease the variance of γ . As a result, the final average steady-state regulator concentration is reached if the system has decreased the variance of γ sufficiently by increasing the rapidity of its response.

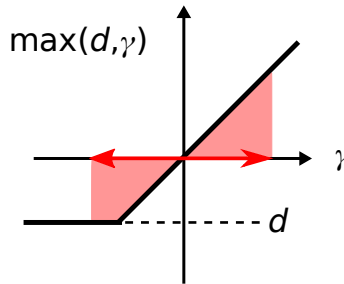


FIG. S2. The nonlinearity in the regulatory architecture. If the fluctuations of the input $\gamma = \sum_i \sigma_{\mu i} (1 - x_i)$ are large enough, the average over the nonlinearity is positive, causing additional growth of the regulator concentration a .

This argument makes it clear why the specific choice of nonlinearity is not particularly important. If $\dot{a} = f(x)$, then the static steady state satisfies $f(x_0) = 0$. For a fast-fluctuating input this becomes

$$\dot{a} = \langle f(x) \rangle = f(x_0) + \frac{1}{2} \langle (x - x_0)^2 \rangle f''(x_0) + \dots$$

For any nonlinear f , as long as $f(x_0) = 0$, the displacement of the original steady state will be determined by higher order statistics of the input. In particular, the rectified-linear nonlinearity in our equations can be replaced, for example, by a Hill function. The system will retain all the relevant behavior as long as the new nonlinearity is \cup -convex in a sufficiently large vicinity of its static fixed point; see section ‘‘A pair of allosteric enzymes’’ for an explicit example.

The assumption $f(x_0) = 0$ is not innocuous; in general, of course, the value of $\langle f(x) \rangle$ is sensitive not only to the variance of x (or other higher-order terms), but also to its mean, and building a system that is sensitive to specifically the variance requires adapting to the mean first. In our model, this is automatically accomplished by the underlying end-product inhibition architecture, which adapts the mean P to mean $D = \bar{D}$, after which x fluctuates around 1, no matter the value of \bar{D} .

S7 The minimal Γ needed to initiate adaptation

Fig. 4A in the main text includes arrows indicating theoretically derived threshold values of Γ above which our system (with a given $\sigma_{\mu i}$) will begin to adapt its timescale of response, deviating from SEPI in its behavior. Here, we show how this threshold value of Γ can be determined.

As discussed in the main text, at static input ($\Gamma = 0$) only N_x out of N_a regulators can be active. Consider the regulators that remain inactive in the static case, and imagine gradually increasing the fluctuation magnitude. Recall the equation for regulator activity dynamics:

$$\tau_a \dot{a}_\mu = a_\mu \max \left(d, \sum_i \sigma_{\mu i} (1 - P_i/D_i) \right) - \kappa a_\mu. \quad (\text{S27})$$

After introducing $\gamma_\mu = \sum_i \sigma_{\mu i} (1 - P_i/D_i)$ we can write

$$\tau_a \dot{a}_\mu = a_\mu (\max(d, \gamma_\mu) - \kappa) = a_\mu \Delta_\mu. \quad (\text{S28})$$

If we chose a_μ as one of the regulators that remained inactive in the static case, we have $\Delta_\mu < 0$ at $\Gamma = 0$; as we begin increasing the fluctuation magnitude, the time-averaged Δ_μ will at first remain negative. The threshold Γ we seek is one where some Δ_μ crosses into positive values. It is clear that if the fluctuations of γ_μ are so small that $\max(d, \gamma_\mu) = \gamma_\mu$ at all times, the system does not adapt. On the other hand, if the fluctuations are large enough and fast compared to the response of the system, they generate an effective additional growth of a_μ . To first order, this additional growth term is proportional to the standard deviation $\sqrt{\omega_\mu}$ of γ_μ . Therefore, we expect the fluctuations to cause a growth of a_μ if the additional growth term is large compared to κ , i.e. $\sqrt{\omega_\mu} \gtrsim c \cdot \kappa$, with c a constant of order 1.

The approximate value of c can be determined using the following argument. With $d = 0$, and assuming that γ_μ is, first, fluctuating on a fast timescale compared to τ_a and, second, is Gaussian with mean $\bar{\gamma}_\mu$ and variance ω_μ , we can average over the fluctuations in Eq. (S28):

$$\langle \Delta_\mu \rangle = \frac{\bar{\gamma}_\mu}{2} + \sqrt{\frac{\omega_\mu}{2\pi}} \exp \left(-\frac{\bar{\gamma}_\mu^2}{2\omega_\mu} \right) + \frac{\bar{\gamma}_\mu}{2} \operatorname{erf} \left(\frac{\bar{\gamma}_\mu}{\sqrt{2\omega_\mu}} \right) - \kappa. \quad (\text{S29})$$

The system is in a stable steady state if either $\langle \Delta_\mu \rangle = 0$ and $a_\mu \geq 0$ or $\langle \Delta_\mu \rangle < 0$ and $a_\mu = 0$. In the non-trivial first case we get the condition $\bar{\gamma}_\mu \leq \kappa$. Approximating $\bar{\gamma}_\mu \approx 0$ one sees that the average growth rate $\langle \Delta_\mu \rangle$ is positive if $\sqrt{\omega_\mu} > \sqrt{2\pi}\kappa$, so that $c = \sqrt{2\pi}$. If this condition is satisfied, a_μ continues its growth until the separation of timescales between γ_μ and τ_a becomes invalid and ω_μ decreases; this is the mechanism by which the system adapts to fast fluctuations.

The variance ω_μ can be derived from the statistical properties of D . If the fluctuations of the demand D are small it holds that $\omega_\mu \approx \delta \hat{D}^T \bar{\sigma}_\mu \delta \hat{D}$ where $\delta \hat{D}$ is the covariance matrix of the stationary probability distribution of the fluctuations $\delta \vec{D}$ with $\langle \delta D_1^2 \rangle = \Gamma \left(\frac{\cos^2 \alpha}{\lambda_1} + \frac{\sin^2 \alpha}{\lambda_2} \right)$ and $\langle \delta D_1 \delta D_2 \rangle = \Gamma \cos \alpha \sin \alpha \left(\frac{\lambda_1 - \lambda_2}{\lambda_1 \lambda_2} \right)$. The variance ω_μ is then given by $\omega_\mu = \bar{\sigma}_\mu^T \delta \hat{D} \bar{\sigma}_\mu$ and the minimal value of Γ is set by the largest ω_μ of the considered system.

S8 Realistic biochemical implementations

In the main text we proposed a simple model of metabolic regulation which highlighted the necessary properties for learning environment statistics, namely an excess of regulators a_μ , self-activation, and a nonlinear regulation of

a_μ by the metabolite concentrations x_i . To show how these properties can enable more realistic systems to learn the statistics of a fluctuating environment, here we present two biochemical implementations. The first of these implements dynamics nearly identical to those described in the main text, and the second, illustrated in Fig. 5b, bears resemblance to two-component systems. As described in the main text, we do not necessarily expect either of these networks to be implemented in real biological systems “as is”. Instead, we use these to illustrate the diversity of systems that could use the logic described in this paper to learn statistics of their environment. For simplicity, we consider the one-dimensional case (first column of Fig. 3 in the main text).

S8.1 A pair of allosteric enzymes

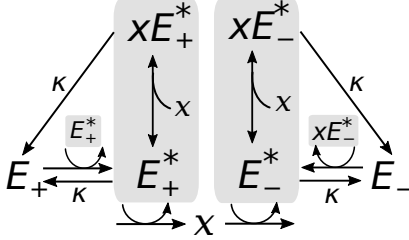


FIG. S3. Implementation of the regulatory mechanism based on a pair of self-activating enzymes which can be in an active (E^*) or inactive state (E). Gray shading indicates catalysts of reactions.

Here, we discuss a realization of our regulatory logic which was not described in the text. This realization of the logic instantiates very similar dynamics to those in the main text, with the nonlinearity taking a more realistic form of a Hill function derived from cooperative binding.

This network is shown in Fig. S3. The enzymes E_+ and E_- can be in an active or inactive state: The active form of E_+ , which we denote E_+^* , catalyzes the production of x ; similarly, E_-^* catalyzes degradation of x . In addition, we postulate that active enzymes can bind to molecules of the metabolite x , which controls self-catalytic activity (see diagram). The total concentration of E_+^* , bound and unbound, plays the role of the activating regulator a_+ from the main text ($a_+ = [E_+^*] + [xE_+^*]$), while E_-^* plays the role of the inhibitor a_- ($a_- = [E_-^*] + [xE_-^*]$).

The same regulatory structure could be realized with transcription factor regulation, with the role of the active enzymes (E_+ and E_-) played by two transcription factors. In this version, activation/deactivation of enzymes is replaced by the simpler process of transcription factor synthesis/degradation. For concreteness, here, we focus on the enzymatic case, largely because we expect architectures like ours to be more relevant in fast-responding circuits, which tend to be non-transcriptional. However, except for the difference of timescales, the dynamics of the two versions would otherwise be identical; in particular, both implementations would “learn” in the same way.

For this discussion, it is convenient to have timescales of dynamics of a_μ and x_i encoded as explicit parameters. Assuming first order kinetics, the dynamics of the network can then be described by:

$$\begin{cases} \tau_x \dot{x} = \gamma_+ a_+ - \gamma_- x a_- - x D(t), \\ \tau_a \dot{a}_+ = a_+ \frac{c_+^n}{c_+^n + x^n} - a_+ \kappa_+, \\ \tau_a \dot{a}_- = a_- \frac{x^m}{c_-^m + x^m} - a_- \kappa_-. \end{cases} \quad (\text{S30})$$

Here, we assume that the metabolite x is much more abundant than the active enzymes E_+^* and E_-^* , meaning that the relative amount of bound x is very small. This allows us to neglect, in the dynamics of x , the source and sink terms due to binding and unbinding of x to the enzymes. We also assume that this binding and unbinding occurs on a much faster timescale than all other processes.

Figure S4 shows an example of simulation results for these dynamics (for the full list of parameters used, see section “Parameters used in figures”). We see that the system reacts to an increasing variance of environmental fluctuations (A) by increasing regulator activities (B). The figure also shows the behavior of a SEPI system which only consists of one a_+ regulator described by the dynamics in Eq. (S30). Fig. S4C shows that the response strength, defined as discussed in the SI section “Defining the system’s responsiveness,”

$$\mathcal{R} = \frac{d\dot{P}}{dD} \approx \gamma_+ a_+ \frac{nc_+^n}{(c_+^n + 1)^2} + \gamma_- a_- \frac{mc_-^m}{(c_-^m + 1)^2}, \quad (\text{S31})$$

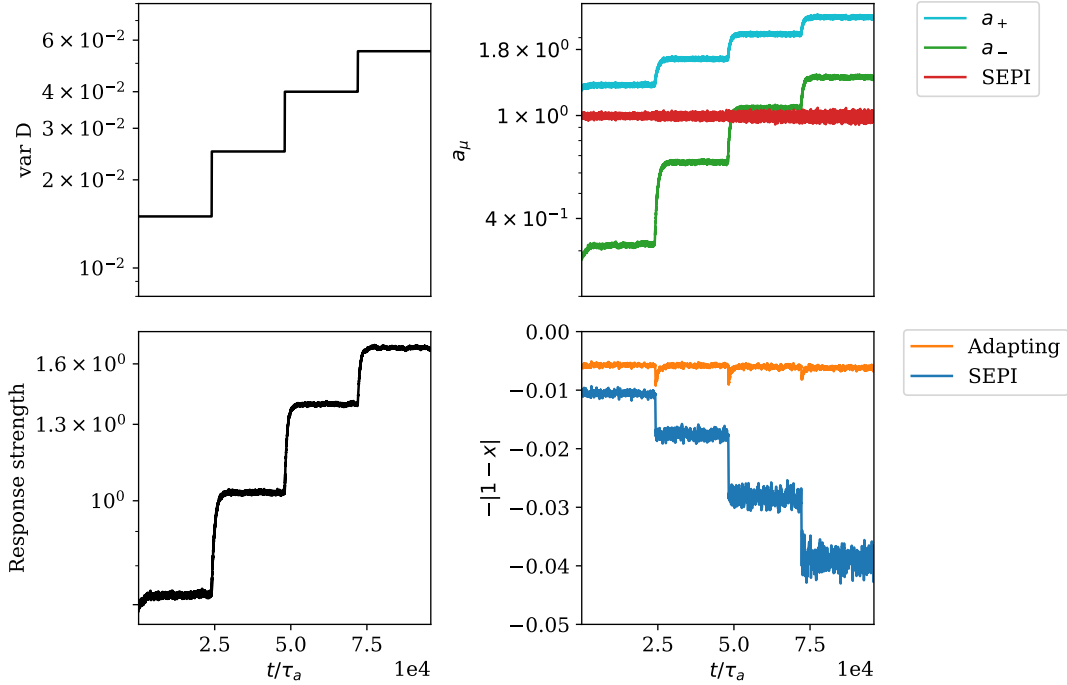


FIG. S4. Adaptation of responsiveness to an increasing variance of environmental fluctuations. A: Step-wise increase of the variance of D . B: Time-series of regulator concentrations, where a_+ and a_- correspond to the total concentrations of t_+ and t_- respectively. C: The responsiveness of the system as defined in Eq. (S31). D: The deviation of the metabolite concentration x from its target value. The panels show averages over 40 realizations.

is increasing due to the changed regulator activities. Finally, Fig. S4D compares the performance of the system Eq. (S30) with the corresponding SEPI system (which, again, we define by the same equations as Eq. (S30), except without the a_- regulator). Similar to Figure 3F in the main text, the performance of the adapting system does not change as the variance of the stimulus increases, while the SEPI system becomes worse.

S8.2 An architecture based on a bifunctional enzyme

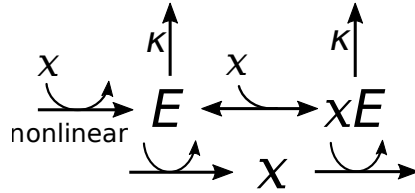


FIG. S5. Regulation by allosteric forms of one enzyme E . The unbound form E activates the production of x , while the bound form xE promotes its degradation. The synthesis of E is regulated nonlinearly by the metabolite concentration x .

In the main text, we presented a network (Fig. 5B) that, despite a lack of obvious similarity to our proposed architecture, contains the same key ingredients and is also able to learn. We described this network’s relationship to two component systems in the main text; here, we will use it to produce an analog of Fig. 3C-F in the main text.

For the reader’s convenience, we reproduce this circuit in Fig. S5 (identical to Fig. 5B in the main text). As described in the main text, for greater generality, we will here rephrase the task: instead of matching production to demand, we will think of maintaining the homeostasis of a quantity x perturbed by external factors. For example, instead of being a metabolite concentration, x could be osmolarity mismatch, and our circuit a hypothetical architecture for active control of osmotic pressure. In this interpretation, the enzyme E might be a mechanosensor triggered by tension in the membrane or cell wall, while “production” and “degradation” of x could be activities of opposing pumps, or

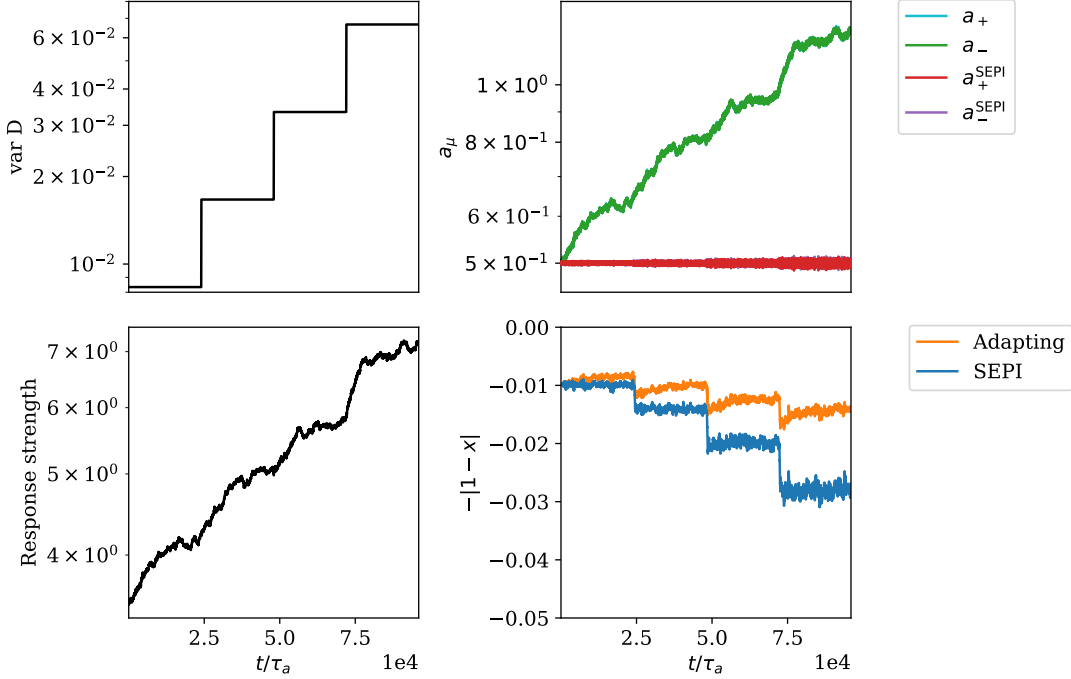


FIG. S6. A: The variance of D is increased step-wise. B: Change of regulator activities. The regulator activities a_+ and a_- overlap strongly and cannot be distinguished in this panel. C: The response strength of the system. D: The mismatch of the metabolite concentration x from its target value. All results show an average over 6 realizations.

regulators of glycerol export or metabolism.

To simplify our language when describing the terms in the specific equations we simulate, we will still talk of a metabolite x being produced and degraded. However, to better accommodate alternative interpretations, the regulator activities will now be defined so that a_+ and a_- would be equal on average (for example, the activities of pumps in opposite directions should, on average, balance). This homeostasis-maintaining formulation is in contrast to Fig. 3D in the main text, where regulators satisfied the constraint $\langle a_+ - a_- \rangle = \bar{D} = 1$.

The production and degradation of x are catalyzed by a bifunctional enzyme that changes its activity when bound to x forming the compound xE . The concentration of the unbound form E corresponds to the activating regulator, $a_+ = [E]$, and increases the production P of x , while xE plays the role of the inhibiting regulator, $a_- = [xE]$, and promotes the degradation of x .

As above, we assume first order kinetics for the production and degradation of x , and that the binding kinetics are fast compared to the other timescales in the problem. Defining $A = a_+ + a_- = [E] + [xE]$ as the total concentration of the enzyme E in both its bound and unbound states, the bound and unbound fractions are described by Hill equations:

$$a_+ = A \frac{c^m}{x^m + c^m}, \quad a_- = A - a_+. \quad (\text{S32})$$

The dynamics of our system are then:

$$\begin{cases} \tau_x \dot{x} = P_0 + \gamma_+ a_+ - \gamma_- x a_- - x D(t) \\ \tau_A \dot{A} = -A \kappa + f(x), \end{cases} \quad (\text{S33})$$

where we assumed that modifying the enzyme E does not significantly affect the quantity x . (In the metabolic formulation, this corresponds to the assumption that x is much more abundant than E , so that the sequestration of x by E has negligible effect on the free concentration of x ; in the osmotic formulation, triggering mechanosensors has negligible effect on pressure itself). In the second equation, the synthesis of the enzyme E depends nonlinearly on the metabolite concentration x . The specific form of nonlinearity does not significantly affect the results, as long as it is sufficiently \cup -convex in the vicinity of the operating point: As described in section “Nonlinearity as a sensor of fluctuation variance” we can think of the nonlinearity $f(x)$ as a “sensor” for the variance of environmental

fluctuations. Whenever fluctuations in $D(t)$ increase such that the current responsiveness of the system fails to maintain the homeostasis of x within previous bounds of fluctuation magnitude, the fluctuations of x will lead to growth of A , increasing the responsiveness until it is again able to reduce the fluctuations of x . In our simulations we chose a Hill function with cooperativity 4 (see section ‘‘Parameters used in figures’’).

Figure S6 shows simulation results for this system. As in the first column of figure 3, the variance of D is increased and the response of the system to this change is monitored. We see that the regulator concentrations correspondingly increase, causing a larger response strength $|\frac{dx}{dx}| \approx 1 + \frac{2\gamma Ec^m m}{(1+c^m)^2}$. The increase in response strength is able to compensate for most of the performance loss, which shows that the system successfully adapts its timescale of response. This is in contrast to the ‘SEPI-like’ system with a fixed value $A = 1$, which cannot adapt its responsiveness and whose performance drops with every increase in fluctuation variance.

S9 Adaptation to static demand

In the main text we argue that the production \vec{P} of the proposed system Eq. (3) adapts to any static demand \vec{D} . The full dynamics of the system is

$$\tau_a \dot{a}_\mu = a_\mu \max \left(d, \sum_i \sigma_{\mu i} (1 - P_i/D_i) \right) - \kappa a_\mu. \quad (\text{S34})$$

With a static demand, Eq. (S34) possesses the same fixed points as the simplified dynamics:

$$\tau_a \dot{a}_\mu = a_\mu \left(\sum_i \sigma_{\mu i} (1 - P_i/D_i) - \kappa \right). \quad (\text{S35})$$

These dynamics have a Lyapunov-function

$$F(\{a_\mu\}) = - \sum_i \frac{1}{2D_i} (P_i - D_i)^2 - \kappa \sum_\mu a_\mu. \quad (\text{S36})$$

This can be verified by considering the temporal change of F

$$\frac{dF}{dt} = \sum_\mu \frac{\partial F}{\partial a_\mu} \frac{da_\mu}{dt} = \sum_\mu a_\mu \Delta_\mu^2 > 0, \quad (\text{S37})$$

with $\Delta_\mu = \sum_i \sigma_{\mu i} (1 - P_i/D_i) - \kappa$. Thus, F always increases and is obviously bound from above. For small κ , the maximum of F is reached for $\vec{P} \approx \vec{D}$, showing that the system adapts to any static demand.

S10 The role of self-activation

In the main text we argue that our proposed system requires three ingredients to adapt to fluctuating environments: excess of regulators with cross-talk, self-activation of regulators and nonlinear activation/repression of the regulators by the metabolite concentrations. Figure 5A shows that excess and nonlinear activation/repression are needed. Here, in Fig. S7 we show that also self-activation is necessary. The plot shows results for the same simulations as in Figure 5A with the difference that this time we omit the prefactor a_μ in front of the max function in the dynamics of the system. In Fig. 5A (with self-activation), for a sufficient number of regulators the performance becomes better with increasing d . In contrast, in Fig. S7 (without self-activation) it becomes worse, showing that the system is not adapting to the fluctuations.

Note that for the SEPI-like case with $N_a = N_x = 2$, the activities of regulators remain approximately constant at $a_\mu = 1$; therefore, in this case, including or omitting the a_μ prefactor results in identical performance. This is why we included a ‘‘SEPI’’ label on Fig. 5A, even though all models included in that parameter sweep had self-activation (and our definition of SEPI does not).

One may note that, unlike the primary architecture we considered in the main text (Fig. 2C), the circuit described in Section S8 S8.2 does not include any explicitly self-catalytic interaction. However, recalling the definitions of $\{a_+, a_-\}$, we can write $a_+ = (a_+ + a_-) \frac{c^m}{x^m + c^m}$ and $a_- = (a_+ + a_-) \frac{x^m}{x^m + c^m}$. Thus, a small change in the concentration x leads to a change in a_+ and a_- which is proportional to the sum of a_+ and a_- . In this way, our bifunctional-enzyme-based circuit also includes an element of self-activation.

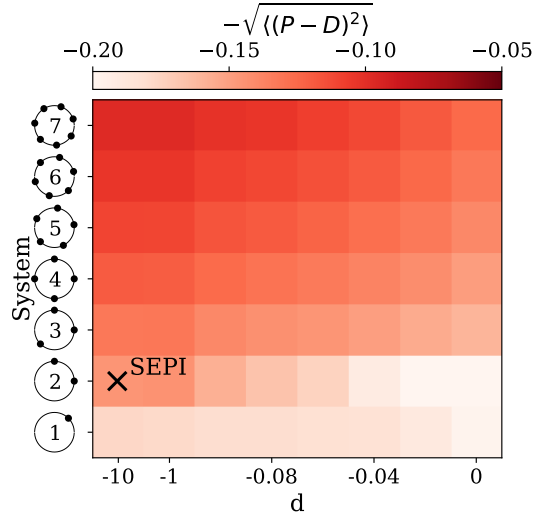


FIG. S7. Reproduction of Figure 5A in the main text without self-activation.

S11 Parameters used in figures

If not stated otherwise we use the following parameters: $\bar{D} = 1$, $\Gamma = 0.35$, $d = 0$, $\kappa = 0.015$, $\tau_a = 3$, $\alpha = 45^\circ$, $\lambda_1 = 8.75$, $\lambda_2 = 875$, $dt = 1/\lambda_2 \approx 1.14 \cdot 10^{-3}$. Since the demand D_i is modelled by a stochastic process which is, in principle, unbound there is a non-zero probability that the demand D_i becomes negative (which is very small for the chosen parameters). To prevent this behavior in the simulations we set $D_i = 0.01$ if $D_i < 0.01$.

Figure 3 C-F:

Fluctuations: In 1D the matrix M only has one element which we set to $M = 7.5$, $\Gamma = [0.048, 0.082, 0.16, 0.3]$.

System: $\kappa = 0.03$.

Timescales: $\tau_a = \tau_a^{SEPI} = 1$.

Average over 80 realizations.

Figure 3F shows a running average over 5 steps.

Figure 3 I-L:

Fluctuations: $\alpha = [-60, 30, -30, 60]$.

System: $N_a = 5$, $\tau_a = 1/\lambda_1$, $\kappa = 0.02$.

SEPI: For a fair comparison, the timescale of SEPI is chosen such that its responsiveness matches the faster responsiveness of the $N_a = 5$ adapting system (measured in an environment with an isotropic M with the same determinant as used in Fig. 3J-L): $\tau_a^{SEPI} = \tau_a/4.9$.

For visualization purposes, to prevent long transients after changes of the activation angle, the regulator activities were capped from below at $a_\mu = 0.1$.

The results are averaged over 40 realizations.

Figure 3L shows a running average over 100 steps.

Figure 4 A:

Fluctuations: Γ from 0 to 0.1 in 40 equidistant steps.

Timescale SEPI: $\tau_a^{SEPI} = \tau_a = 3$.

Simulation length: $5 \cdot 10^7$ steps.

Figure 4 B:

Fluctuations: $\Gamma = 0.05$,

anisotropy $A = [1, 1.05, 1.1, 1.15, 1.2, 1.25, 1.3, 1.35, 1.4, 1.45, 1.5, 1.55, 1.6, 1.65, 1.7, 1.75, 1.8, 1.85, 1.9, 1.95, 2, 2.1, 2.2, 2.3, 2.4, 2.5, 2.6, 2.7, 2.8, 2.9, 3.25, 3.5, 4, 4.5, 5, 6, 7, 8, 9, 10]$. For each value of A λ_1 and λ_2 are chosen as:

$\lambda_1 = \frac{1+A^2}{rA^2}$, $\lambda_2 = A^2\lambda_1$ with $r = 1/8.75 + 1/875$.

Timescale SEPI: $\tau_a^{SEPI} = \tau_a = 3$.

Simulation length: $5 \cdot 10^7$ steps.

Figure 5 A:

Fluctuations: Results averaged over activation angles $\alpha = [45, 85, 125, 165, 205]$.

System: $\kappa = 0.02$, $\tau_a = 1/\lambda_1$.

Simulation length: 10^7 steps.

Figure S1:

System: κ from 0.01 to 0.025 in steps of size $1.25 \cdot 10^{-4}$.

Simulation length= $5 \cdot 10^7$ steps.

For each simulation, the performance was averaged over the last 10^7 time steps.

Figure S1 inset:

All system parameters as in Figure S1 except for: κ from 0.013 to 0.014 in steps of size $2.5 \cdot 10^{-5}$.

Simulation length: 10^8 steps.

For each simulation, the performance was averaged over the last $2 \cdot 10^7$ steps.

The results are binned in 20 equal-width bins.

Figure S4:

The parameters in the simulation were chosen so as to ensure that, first, $\tau_x \ll \tau_a$; and second, the steady-state x stays at 1 (this is analogous to setting $x_0 = 1$ in the main text). Specifically, we used: $\tau_x = 0.01$, $\tau_a = 1$, $\gamma_+ = \gamma_- = 1$, $n = 2$, $m = 2$, $c_+^n = 0.5$, $c_-^m = 2$, $\kappa_+ = 1.0025 \frac{1}{c_+^n + 1}$, $\kappa_- = 1.0025 \frac{c_-^m}{c_-^m + 1}$. The parameters describing the fluctuations of D are chosen as: $\bar{D} = 1$, $M = 1$, $\Gamma = [0.015, 0.025, 0.04, 0.055]$.

A brief explanation: While the parameter list is long, there is a simple reasoning which sets most of these choices, and explains how the parameters of this model need to be related to each other in order for the adaptation of responsiveness to occur. First of all, we assume that the concentration x changes on a much faster timescale than the regulator concentrations a ; here we choose $\tau_a = 1$ and $\tau_x = 0.01$. Further, the average of $D(t)$ is chosen to be equal to one. Then, for small fluctuations of D we have $x \approx \gamma(a_+ - a_-)$. On the other hand, the non-trivial fixed points of the regulator concentration dynamics are reached if

$$\frac{c_+^n}{c_+^n + x^n} = \kappa_+ \quad \text{and} \quad \frac{x^m}{c_-^m + x^m} = \kappa_- . \quad (\text{S38})$$

Thus, we can set the equilibrium point of x by choosing κ_+ , κ_- , c_+ and c_- . Here, without loss of generality, we choose that the fixed point is reached at $x = x_0 = 1$ by setting

$$\frac{c_+^n}{c_+^n + 1} = \kappa_+ \quad \text{and} \quad \frac{1}{c_-^m + 1} = \kappa_- . \quad (\text{S39})$$

For the sought-after effect to occur, the fast fluctuations of x around $x_0 = 1$ need to result in an effective additional growth of a_+ and a_- , providing a ‘‘sensor’’ for the variance of D . One possibility to get this behavior is to set $c_-^m = 2$ and $c_+^n = 0.5$. To avoid the regulator concentrations to grow indefinitely, κ_+ and κ_- need to be a little larger than the determined values in Eq. (S39). Finally, the parameter γ can be chosen rather freely; here we choose $\gamma = 1$. Simulation length: $3.2 \cdot 10^7$ steps with $dt = 3 \cdot 10^{-3}$. Panel D shows a running average over 50 timesteps.

Figure S6:

We used the following parameters for the simulations: $\tau_x = 1$, $\tau_A = 25$, $P_0 = 1$, $\gamma_+ = \gamma_- = 5$, $\kappa = 10^{-3}$, $c^m = 1$, $m = 1$. The nonlinearity was chosen as: $f(x) = d \frac{x^n}{x^n + c_1^n} - \beta$ with $d = 10$, $c_1^n = 10$, $n = 4$, $\beta = 5 \cdot 10^{-4}$. The parameters describing the fluctuations of D are set to: $M = 3$, $\Gamma = [0.025, 0.05, 0.1, 0.2]$. For the mechanism to work, the timescales need to fulfill $\tau_A \gg \tau_x$. The parameters P_0 , m and c are set by the choice of the fixed-point x_0 (here $x_0 = 1$). Simulation length: $3.2 \cdot 10^7$ steps with $dt = 3 \cdot 10^{-3}$. Panel D shows a running average over 100 timesteps.

Figure S7: Same parameters as in Figure 5A.